Instrument Science Report COS 2010-08

SMOV: COS NUV External Spectroscopic Performance

Stéphane Béland[1] & Parviz Ghavamian[2]

[1] University of Colorado at Boulder
[2] Space Telescope Science Institute, Baltimore, MD

September 30, 2010

ABSTRACT

We present the results from two COS SMOV programs (COS16 and COS17) designed to measure the spectral and spatial resolution of the COS NUV channel. The measured spectral resolution of data acquired through the PSA and BOA aperture match the requirements from the CEI specifications for COS. Observations from other SMOV programs were also utilized to increase the wavelength coverage and the number of isolated spectral lines available for analysis. The spectral resolution degradation as the target is displaced 0.25" from the center of the aperture was estimated to be around 29% and 21% for the G185M and G225M. Definitive measurements could not be made for the G285M and G230L gratings from the data. The plate scales were also determined for each grating in the dispersion and cross-dispersions. The spatial resolution for the PSA aperture was then obtained using the resulting plate scale and found to be: 0.075"± 0.004" (G185M), 0.058"± 0.002" (G225M), 0.056" ± 0.001" (G285M) and 0.081" ± 0.001" (G230L). The corresponding BOA spatial resolution is 0.29″, 0.22″, 0.24″ and 0.38″ for G185M, G225M, G285M and G230L, respectively. The aperture throughput along dispersion and perpendicular to dispersion was also determined as a function of the position of the target relative to the center of the PSA.

Contents:

1. Introduction and Overview

The Cosmic Origins Spectrograph (COS) was installed on HST during the Servicing Mission 4 on May 16 2009. A series of calibration and characterization plans were developed and executed during the Servicing Mission Observatory Verification (SMOV). This ISR covers the Near UV (NUV) External Spectroscopic Performance of COS (COS SMOV Programs 16 and 17). The performance was assessed by measuring the **spectral** resolution from absorption lines and **spatial** resolution from emission lines of targets observed through both the PSA and BOA apertures. The other goals of these programs were to determine the on-orbit plate scale of the COS NUV channel, to measure the aperture throughput as a function of off-axis position, and to measure the interdependence (if any) between the spectral and spatial resolution of the detector.

COS NUV spectra acquired through the Primary Science Aperture (PSA) were designed to cover the 1750 Å – 3200 Å spectral range at spectroscopic resolving powers, R ($\equiv \lambda/\Delta\lambda_{FWHM}$) of R > 20,000 for the G225M and G285M gratings, R > 16,000 for the G185M and R > 2000 for the G230L grating. According to the Contractual End Item (CEI) specifications for COS, the spectral resolution must be achieved over 80% of the usable bandpass.

2. NUV Spectral Resolution: Ground Testing

The NUV Primary Science Aperture (PSA) spectral resolution was measured during the 2003 and 2006 thermal-vacuum testing of the instrument using an external PtNe

calibration lamp at every central wavelength setting of every NUV grating. The width of a best-fit Gaussian was used to measure the resolution of isolated PtNe spectral lines. The resolution was determined to meet the CEI requirements for all gratings.

During thermal-vacuum testing, the Bright Object Aperture (BOA) was used only in imaging mode. Therefore, the spectral resolution of the BOA was estimated indirectly by first comparing the relative degradation of the point-spread-function (PSF) of PSA imaging data with the PSF of the BOA imaging data, then applying that degradation to the PSA spectral resolution obtained from spectroscopic data.

3. On-orbit characterization of COS NUV Spectral Resolution

The SMOV program COS-16 (program ID 11476), "NUV External Spectroscopic Performance – Part 1", was designed to characterize the on-orbit spectral resolution for the NUV gratings.

3.1 Target Selection

The primary target for this program with the PSA, is the subdwarf B star Feige 48 (PG 1144+651). This star has been observed with the STIS high resolution echelle grating and narrow slit showing numerous unresolved absorption features. The BOA observations used the bright O subdwarf BD+75°325, a bright HST calibration standard.

From high signal-to-noise HST/STIS and FUSE data, Herber et al. (2000) and O'Toole et al. (2004), determined that Feige 48 is a binary system with a velocity semi-amplitude K=28.0±0.2 km/s for the sdB component and an orbital period of P_{orb}=9.024±0.072 hours for the system. The orbital inclination is estimated at $\leq 11.4°$ ($V \sin i \leq 5$ km/s). This has the potential of broadening the narrow spectral lines and reducing the measured spectral resolution. The exposures for all FP-POS for each grating were taken within about 0.5 hour which still corresponds to a maximum position shift between the first and last FP-POS exposures of 10 km/s or about 2 pixels (0.8 resolution element). Because of this significant effect, the different FP-POS were analyzed individually and not combined. This introduced a smear of no more than 2.6 km/s or 0.5 pixel. By using a single FP-POS, we minimized the smear from the orbital motion at the cost of lower signal-to-noise, reducing the spectral resolution measurements to the strongest lines only.

3.2 Data Acquisition

Spectra of Feige 48 were obtained through the PSA with the G185M, G225M, G285M and G230L gratings (at 1850 Å, 2250 Å, 2695 Å and 3000 Å central wavelengths respectively). All observations were done in time-tag mode with tagflash enabled. After a target acquisition was performed to center the target in the center of the aperture, an exposure was taken at all four FP-POS positions. Typical exposure times for each FP-

POS were t_{exp} = 150s for G185M and G225M, t_{exp} = 350s for G285M, and t_{exp} = 120s for G230L. Four additional exposures were taken, offset by 0.25 arcseconds from the center of the aperture in a diamond pattern, each of these at two FP-POS (1 and 3). For the G185M at 1850 Å, a time-tag exposure with FLASH=NO was obtained to verify the auto-wavecal capability of the NUV channel.

The BOA observations, with BD+75°325, were done at 1864 Å, 2268 Å, 2617 Å and 3360 Å for the four gratings respectively. The observations were done in time-tag mode with FP-POS=AUTO (all four positions). All BOA observations were performed with the target centered in the aperture.

3.3 Data Analysis

3.3.1 Primary Science Aperture (PSA)

It was reported in the COS Instrument Science Report "Preliminary Characterization of the Post-Launch Line Spread Function of COS" (Ghavamian et al. 2009), that the Line Spread Function for the NUV detector shows extended wings and reduced central intensity compared to profiles measured in ground testing. These wings are attributed to the mid-frequency wave-front errors (MFWFE) on the mirrors of HST. The flux in those wings was shown to decrease with increasing wavelength. This flux redistribution was estimated to be about 30% for the G185M and 20% for the G225M and G285M.

For our program, Gaussian profiles were fitted to the data and no attempt was made to use the modeled LSF for the NUV detector. Although fitting Gaussians will introduce a small error in line width and flux, the resolution measurement errors were dominated by such factors as the difficulty in fitting a Gaussian to the data due to low signal-noise, the ability to determine the continuum, and errors in identifying non-blended spectral features.

For the absorption lines, the continuum was determined from the surrounding signal by fitting either a linear or a second order polynomial. A Gaussian function was used to fit the spectral profiles. The signal-to-noise ratios of the Feige 48 spectra varied between 8 and 10 for the individual exposures, and only a few lines have been determined to have enough signal and to be sufficiently isolated to get reliable resolution measurements. Additional observations obtained as part of other SMOV programs were also used to measure the resolution over a wider spectral coverage. Table 3-1 lists the files and spectral lines used for this program. Figure 3-1 shows the measured resolution versus wavelength from Table 3-1. Note that there is a scatter in values of R, due in part to uncertainties in determining the exact placement of the continuum. This makes some resolution values in Tables 3-1 and Figure 3-1 appear very large, R > 30,000.

Table 3-1 Filenames and targets used for the NUV resolution measurement.

Program	Filename	Target	Grating	CW	APT	Stripe	Line CW	Line FWHM	Resolution
11476	laaq01qpq	Feige48	G185M	1850	PSA	NUVA	1745.4404	0.08290442	23887.4
11476	laaq01qpq	Feige48	G185M	1850	PSA	NUVA	1745.44	0.0762	22906.0
11476	laaq01qlq	Feige48	G185M	1850	PSA	NUVA	1767.6116	0.12535008	14101.4
11476	laaq01qlq	Feige48	G185M	1850	PSA	NUVA	1767.61	0.1255	14186.3
11476	laaq01qjq	Feige48	G185M	1850	PSA	NUVA	1769.3063	0.11706493	13369.1
11476	laaq01qjq	Feige48	G185M	1850	PSA	NUVA	1769.31	0.1224	14455.1
11476	laaq01qpq	Feige48	G185M	1850	PSA	NUVB	1838.09	0.1071	17162.4
11476	laaq01qpq	Feige48	G185M	1850	PSA	NUVB	1838.0910	0.09937115	18497.2
11476	laad01knq	Feige48	G185M	1786	PSA	NUVB	1854.6485	0.11764454	15764.9
11476	laaq01qpq	Feige48	G185M	1850	PSA	NUVB	1862.5533	0.09988494	18647.0
11476	laaq01qpq	Feige48	G185M	1850	PSA	NUVB	1862.55	0.1038	17943.6
11476	laaq01qpq	Feige48	G185M	1850	PSA	NUVB	1866.0874	0.11778722	20796.7
11476	laaq01qpq	Feige48	G185M	1850	PSA	NUVB	1866.08	0.0787	23711.3
11476	laad01klq	Feige48	G185M	1786	PSA	NUVC	1895.3951	0.081007878	23397.6
11476	laaq01qjq	Feige48	G185M	1850	PSA	NUVC	1950.0516	0.12644499	16180.7
11476	laaq01qjq	Feige48	G185M	1850	PSA	NUVC	1950.05	0.1200	16250.4
11476	laaq01qlq	Feige48	G185M	1850	PSA	NUVC	1957.6781	0.15351452	12752.4
11476	laaq01qlq	Feige48	G185M	1850	PSA	NUVC	1957.67	0.1516	12913.4
11476	laaq01qlq	Feige48	G185M	1850	PSA	NUVC	1965.0363	0.08764200	22421.2
11476	laaq01qjq	Feige48	G185M	1850	PSA	NUVC	1965.0295	0.14677440	18746.7
11476	laaq01r6q	Feige48	G185M	1850	PSA	NUVC	1965.17	0.0865	22718.7
11476	laaq01qjq	Feige48	G185M	1850	PSA	NUVC	1966.47	0.0900	21849.7
11476	laaq01qjq	Feige48	G185M	1850	PSA	NUVC	1966.4639	0.09088038	21637.9
11481	la9g01msq	G191-B2B	G185M	1850	PSA	NUVA	1752.4869	0.08611051	20351.7
11481	la9g01msq	G191-B2B	G185M	1850	PSA	NUVB	1854.6288	0.10139890	18290.4
11476	laaq01rvq	Feige48	G225M	2250	PSA	NUVA	2143.9574	0.08409000	25494.2
11476	laaq01s3q	Feige48	G225M	2250	PSA	NUVA	2152.2043	0.088529584	24310.6
11476	laaq01s3q	Feige48	G225M	2250	PSA	NUVA	2152.20	0.0867	24823.6
11476	laaq01rvq	Feige48	G225M	2250	PSA	NUVA	2158.1779	0.10913460	19775.4
11476	laaq01s3q	Feige48	G225M	2250	PSA	NUVA	2161.69	0.0846	25551.9
11476	laaq01ryq	Feige48	G225M	2250	PSA	NUVA	2167.4066	0.10086670	21487.8
11476	laaq01ryq	Feige48	G225M	2250	PSA	NUVA	2167.40	0.1017	21311.7
11476	laaq01ryq	Feige48	G225M	2250	PSA	NUVB	2251.9078	0.11644336	19339.1
11476	laaq01ryq	Feige48	G225M	2250	PSA	NUVB	2251.88	0.0656	34327.0
11476	laaq01ryq	Feige48	G225M	2250	PSA	NUVC	2339.4225	0.08352198	28009.7
11476	laaq01s3q	Feige48	G225M	2250	PSA	NUVC	2353.03	0.0827	28452.2
11474	labq01keq	HD187691	G225M	2250	PSA	NUVA	2144.6424	0.080974396	26485.4
11474	labq01keq	HD187691	G225M	2250	PSA	NUVB	2235.6234	0.10826444	20649.7
11474	labq01keq	HD187691	G225M	2250	PSA	NUVB	2248.0003	0.073885161	30423.6
11474	labq01koq	HD187691	G225M	2186	PSA	NUVB	2177.6178	0.094888569	22949.1
11474	labq01koq	HD187691	G225M	2186	PSA	NUVB	2181.8927	0.088930355	24534.8
11474	labq01kqq	HD187691	G225M	2217	PSA	NUVB	2215.5523	0.090298139	24536.0
11474	labq01kqq	HD187691	G225M	2217	PSA	NUVB	2233.6695	0.093060647	23862.5
11474	labq01kqq	HD187691	G225M	2217	PSA	NUVC	2309.3131	0.088825504	25998.3
11474	labq01kqq	HD187691	G225M	2217	PSA	NUVC	2324.4403	0.096496969	24095.0
11474	labq01kyq	HD187691	G225M	2306	PSA	NUVC	2414.9009	0.097822564	24686.6
11474	labq01l4q	HD187691	G225M	2357	PSA	NUVB	2372.8780	0.077365005	30671.2
11474	labq01l4q	HD187691	G225M	2373	PSA	NUVB	2372.2303	0.113126050	20969.8
11474	labq01l6q	HD187691	G225M	2373	PSA	NUVC	2465.7381	0.092715549	26594.7
11474	labq01lcq	HD187691	G225M	2373	PSA	NUVC	2498.1059	0.083152800	30042.3
11474	labq01leq	HD187691	G225M	2373	PSA	NUVC	2496.3579	0.083850778	29771.4
11474	labq74s9q	Feige48	G225M	2217	PSA	NUVA	2107.84	0.0998	21120.1
11474	labq74s7q	Feige48	G225M	2186	PSA	NUVA	2101.54	0.0943	22285.7
11474	labq74s7q	Feige48	G225M	2186	PSA	NUVB	2171.64	0.0884	24566.1
11474	labq74s7q	Feige48	G225M	2186	PSA	NUVB	2181.01	0.0880	24784.1
11474	labq74s7q	Feige48	G225M	2186	PSA	NUVC	2273.92	0.0773	29416.8
11474	labq74sdq	Feige48	G225M	2373	PSA	NUVA	2276.94	0.104	21893.7
11474	labq74sdq	Feige48	G225M	2373	PSA	NUVB	2374.09	0.1154	20572.7
11474	labq74sdq	Feige48	G225M	2373	PSA	NUVB	2390.06	0.0998	23948.5
11474	labq74sdq	Feige48	G225M	2373	PSA	NUVC	2483.58	0.1066	23298.1
11474	labq74sbq	Feige48	G225M	2339	PSA	NUVA	2244.64	0.0937	23955.6

11474	labq74sbq	Feige48	G225M	2339	PSA	NUVB	2325.3868	0.103753	22402.6
11474	labq74sbq	Feige48	G225M	2339	PSA	NUVB	2325.39	0.0985	23608.0
11474	labq74sfq	Feige48	G225M	2410	PSA	NUVA	2325.40	0.1046	22231.4
11474	labq74sfq	Feige48	G225M	2410	PSA	NUVB	2419.1	0.0896	26998.9
11474	labq74sfq	Feige48	G225M	2410	PSA	NUVB	2419.09	0.10216	23678.5
11476	laaq01rtq	Feige48	G225M	2250	PSA	NUVC	2339.47	0.09128	25629.6
11476	laaq01thq	Feige48	G285M	2695	PSA	NUVC	2715.1779	0.089505945	30335.2
11474	labq01hvq	HD187691	G285M	2676	PSA	NUVA	2553.0955	0.084151450	30339.3
11474	labq01hvq	HD187691	G285M	2676	PSA	NUVA	2568.0714	0.099497465	25810.4
11474	labq01hvq	HD187691	G285M	2676	PSA	NUVA	2573.9296	0.094777422	27157.6
11474	labq01hvq	HD187691	G285M	2676	PSA	NUVB	2655.9197	0.083264400	31897.4
11474	labq01hvq	HD187691	G285M	2676	PSA	NUVB	2675.7912	0.080500408	33239.4
11474	labq01hvq	HD187691	G285M	2676	PSA	NUVC	2782.6431	0.091820812	30305.1
11474	labq02o5q	HD6655	G285M	2996	PSA	NUVA	2885.11	0.0969	29774.1
11474	labq02o5q	HD6655	G285M	2996	PSA	NUVA	2874.81	0.0976	29455.0
11474	labq02o5q	HD6655	G285M	2996	PSA	NUVA	2878.97	0.1143	25187.8
11474	labq02o5q	HD6655	G285M	2996	PSA	NUVB	2992.12	0.1254	23854.9
11474	labq02o5q	HD6655	G285M	2996	PSA	NUVB	2997.02	0.1067	28088.0
11474	labq02o5q	HD6655	G285M	2996	PSA	NUVC	3126.34	0.1328	23541.0
11474	labq01jqq	HD187691	G285M	3035	PSA	NUVB	3050.1704	0.094188965	32383.5
11474	labq70rlq	Feige48	G230L	2950	PSA	NUVB	2799.89	1.223	2289.4
11474	labq70rlq	Feige48	G230L	2950	PSA	NUVB	2792.69	1.246	2241.3
11474	labq02mjq	HD6655	G230L	2950	PSA	NUVB	2833.0448	1.09359	2590.6
11474	labq02mjq	HD6655	G230L	2950	PSA	NUVB	2951.3948	1.18187	2497.2
11474	labq03q4q	NGC6833	G230L	2950	PSA	NUVB	2799.4772	1.3735	2038.2
11474	labq03q2q	NGC6833	G230L	2635	PSA	NUVB	2596.4785	1.0913	2379.3
11474	labq03q2q	NGC6833	G230L	2635	PSA	NUVB	2799.8656	1.5070	1857.9
11479	laad02foq	GD71	G230L	3360	PSA	NUVA	2239.8714	0.9823	2280.2
11896	lbbd01hvq	WD1057+719	G230L	2950	PSA	NUVB	2799.7963	0.8833	3169.7
11896	lbbd01hvq	WD1057+719	G230L	2950	PSA	NUVB	3005.5441	1.3350	2251.3
11476	laaq02uuq	Feige48	G230L	3000	PSA	NUVA	1757.8142	1.0547	1715.4
11477	labm02wcq	HE-2-38	G230L	2950	PSA	NUVA	1889.4735	1.1830	1597.2
11477	labm02wcq	HE-2-38	G230L	2950	PSA	NUVA	1906.1203	1.2097	1575.7
11477	labm02wcq	HE-2-38	G230L	2950	PSA	NUVB	2794.5846	1.4906	1874.8
11477	labm02wcq	HE-2-38	G230L	2950	PSA	NUVB	2801.6182	1.2575	2227.9
11477	labm02wcq	HE-2-38	G230L	2950	PSA	NUVB	3045.6702	1.2146	2507.5
11477	labm02wcq	HE-2-38	G230L	2950	PSA	NUVB	3131.5340	1.2248	2556.8

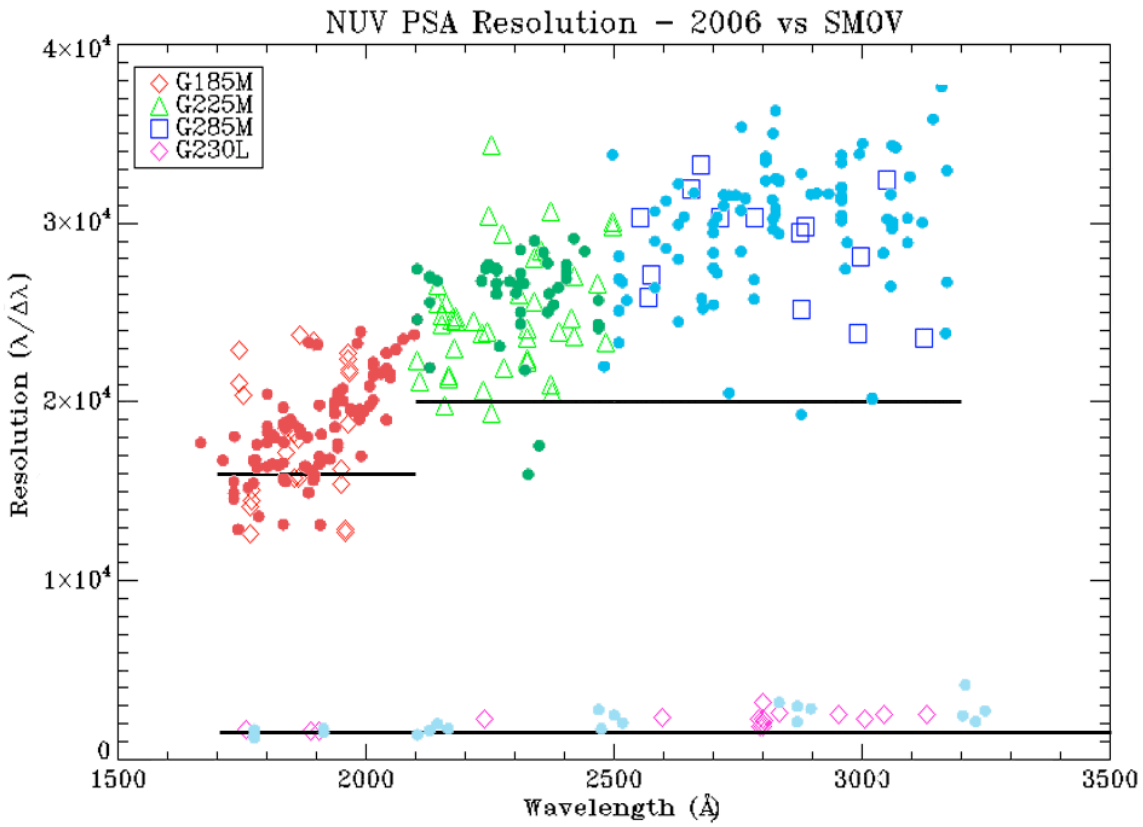

Figure 3-1 Spectral resolution as a function of wavelength for the NUV modes. G185M is in red, G225M is in green, G285M is in blue, and G230L is in light blue. The solid lines indicate the bandpass and spectral resolution requirement for each channel. The solid symbols are from Thermal-Vac 2006 and the open symbols are from this SMOV program.

3.3.2 Bright Object Aperture (BOA)

The data from the Bright Object Aperture exposures are of particularly low signal-to noise ratio (~5-10), hence we used the high resolution STIS spectra of BD+75°325 to aid our identification of good line candidates. We first identified broad spectral features in the BOA spectra, then measured their FWHM and deduced the COS spectral resolving power indirectly by subtracting the line widths from the STIS spectra in quadrature from the widths observed in the COS BOA spectra. Assuming Gaussian spectral features, we can write:

$$\sigma_{obs}(COS)^2 = \sigma_{inst}(COS)^2 + \sigma_{obs}(source)^2 \qquad (1)$$

$$\sigma_{obs}(STIS)^2 = \sigma_{inst}(STIS)^2 + \sigma_{obs}(source)^2 \qquad (2)$$

where:

σ_{obs}(COS) is the FWHM of the feature observed by COS

σ_{inst}(COS) is the COS instrumental FWHM (width of an unresolved feature)

σ_{obs}(STIS) is the FWHM of the feature observed by STIS

σ_{inst}(STIS) is the STIS instrumental FWHM (width of an unresolved feature)

σ_{obs}(source) is the intrinsic FWHM of the emission or absorption feature

By substituing σ_{obs}(source) in Equation (2) into the same term in Equation (1), we get:

$$\sigma_{inst}(COS)^2 = \sigma_{obs}(COS)^2 - \sigma_{obs}(STIS)^2 + \sigma_{inst}(STIS)^2 \qquad (3)$$

The STIS spectra were taken with the E140M and E230M and both have an instrumental profile of about 1.2 pixels in the wavelength range covered by our COS spectra. The E140M and E230M STIS data was taken from program 8635, observed for U. Heber in Feb., 2004 (files o64002010 and o64002030). Table 3-2 lists the files and COS spectra used, along with the resulting resolutions measured using equation 3 above. Figure 3-2 shows the calculated resolution as a function of wavelength for the BOA.

Table 3-2 Filenames and targets used for the NUV resolution measurement.

Program	Filename	Target	Grating	CW	APT	Stripe	Line CW	Line FWHM	Resolution
11476	laaq03010	BD75D325	G185M	1864	BOA	NUVA	1747.3539	0.688936120	2536.5
11476	laaq03010	BD75D325	G185M	1864	BOA	NUVA	1777.2784	0.560642220	3170.1
11476	laaq03010	BD75D325	G185M	1864	BOA	NUVC	1966.5998	0.425404930	4622.9
11476	laaq03020	BD75D325	G225M	2268	BOA	NUVA	2163.9768	0.45738158	4731.2
11476	laaq03020	BD75D325	G225M	2268	BOA	NUVC	2374.2383	0.33699694	7045.2
11476	laaq03020	BD75D325	G225M	2268	BOA	NUVC	2382.5913	0.41131941	5792.6
11476	laaq03030	BD75D325	G285M	2617	BOA	NUVA	2517.7596	0.52257555	4818.0
11476	laaq03030	BD75D325	G285M	2617	BOA	NUVC	2599.9131	0.32998364	7878.9
11474	labq01juq	HD187691	G285M	3035	BOA	NUVB	3051.5064	0.4598094	6636.5
11476	laaq03040	BD75D325	G230L	3360	BOA	NUVA	2248.9821	6.7759030	331.9
11476	laaq03040	BD75D325	G230L	3360	BOA	NUVA	2302.5556	9.9163900	232.2
11476	laaq03040	BD75D325	G230L	3360	BOA	NUVA	2382.0336	9.8759799	241.2

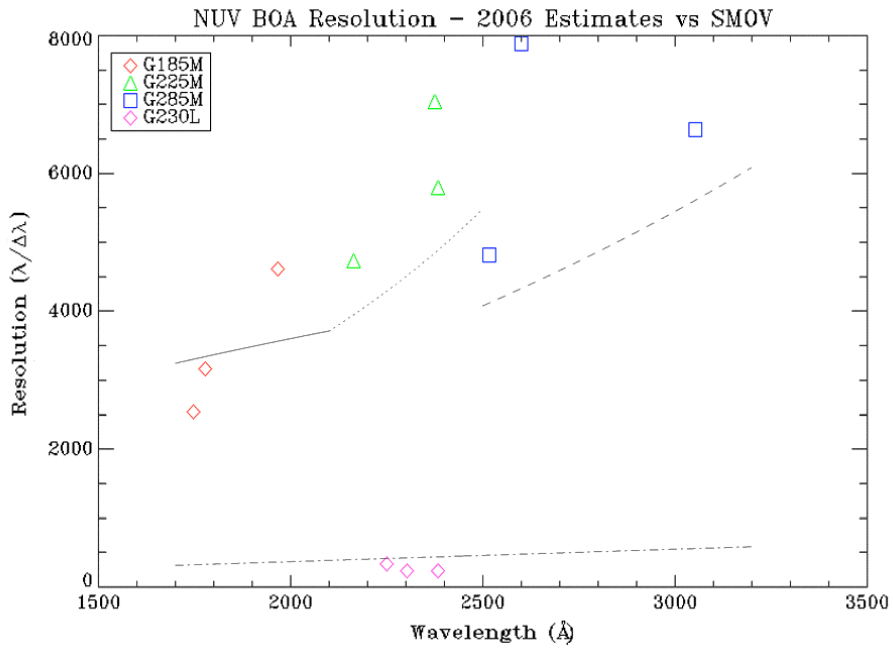

Figure 3-2 Spectral resolution of the NUV using the BOA. The lines correspond to the resolution determined from Thermal-Vac 2006 and the open symbols show the resolution measured in this SMOV program.

4. Spectral Resolution Degradation with Target Misalignment

Additional observations were taken with the target (Feige 48) offset from the center of the PSA by 0.25 arc-sec in a diamond pattern to measure the degradation of the spectral resolution with the target misaligned. These observations were taken at only one central wavelength setting and at only two FP-POS positions. To improve the S/N ratio, the data from all 8 exposures for a single grating (including all POSTARG positions) were combined. Each of the spectra was cross-correlated and aligned with the first dataset before combining them. For the POSTARGs specified along dispersion, this eliminates any possible spectral feature broadening due to the target displacement along dispersion (see Section 5). Note that a misalignement of the target in the PSA would not be visible in wavelength calibration spectra. We used the same set of identified spectral lines used above, for these measurements. The results (shown in Figure 4-1) indicate that the spectral resolution degrades by approximately 29% for the G185M and 21% for the G225M grating.

The number of absorption lines in the spectrum of Feige 48 decreases as the wavelength increases. No useful spectral lines were found in the wavelength ranges covered by the G285M or G230L gratings. However, at off-center positions in the PSA we expect the spectral resolution of data taken with these gratings to degrade in a similar manner to the G185M and G225M gratings.

Table 4-1 Filenames used for the NUV Offset resolution measurement.

Program	Filename	Target	Grating	CW	FP-POS	Offset Disp,XDisp
11476	laaq01raq	Feige48	G185M	1850	3	0.25,0.00
11476	laaq01rcq	Feige48	G185M	1850	1	0.25,0.00
11476	laaq01req	Feige48	G185M	1850	3	0.00,0.25
11476	laaq01rgq	Feige48	G185M	1850	1	0.00,0.25
11476	laaq01riq	Feige48	G185M	1850	3	-0.25,0.00
11476	laaq01rkq	Feige48	G185M	1850	1	-0.25,0.00
11476	laaq01rmq	Feige48	G185M	1850	3	0.00,-0.25
11476	laaq01roq	Feige48	G185M	1850	1	0.00,-0.25
11476	laaq01s5q	Feige48	G225M	2250	1	0.00,-0.25
11476	laaq01s7q	Feige48	G225M	2250	3	0.25,0.00
11476	laaq01saq	Feige48	G225M	2250	1	0.25,0.00
11476	laaq01scq	Feige48	G225M	2250	3	0.00,0.25
11476	laaq01t3q	Feige48	G225M	2250	1	0.00,0.25
11476	laaq01t5q	Feige48	G225M	2250	3	-0.25,0.00
11476	laaq01t7q	Feige48	G225M	2250	1	-0.25,0.00
11476	laaq01taq	Feige48	G225M	2250	3	0.00,-0.25
11476	laaq01trq	Feige48	G285M	2695	1	0.00,-0.25
11476	laaq01ttq	Feige48	G285M	2695	3	0.25,0.00
11476	laaq01twq	Feige48	G285M	2695	1	0.25,0.00
11476	laaq01u1q	Feige48	G285M	2695	3	0.00,0.25
11476	laaq01ufq	Feige48	G285M	2695	1	0.00,0.25
11476	laaq01ukq	Feige48	G285M	2695	3	-0.25,0.00
11476	laaq01umq	Feige48	G285M	2695	1	-0.25,0.00
11476	laaq01uoq	Feige48	G285M	2695	3	0.00,-0.25
11476	laaq02vpq	Feige48	G230L	3000	3	0.00,-0.25
11476	laaq02vrq	Feige48	G230L	3000	1	0.25,0.00
11476	laaq02vtq	Feige48	G230L	3000	3	0.25,0.00
11476	laaq02vvq	Feige48	G230L	3000	1	0.00,0.25
11476	laaq02vxq	Feige48	G230L	3000	3	0.00,0.25
11476	laaq02vzq	Feige48	G230L	3000	1	-0.25,0.00
11476	laaq02w1q	Feige48	G230L	3000	3	-0.25,0.00
11476	laaq02w3q	Feige48	G230L	3000	1	0.00,-0.25

Table 4-2 Measured spectral resolution with 0.25" offset and centered.

Program	Filename	Target	Grating	CW	Stripe	Line CW	Line FWHM	Resolution at 0.25″ offset	Resolution Centered
11476	laaq01_G185	Feige48	G185M	1850	NUVA	1745.4323	0.12837190	13596.7	23396.7
11476	laaq01_G185	Feige48	G185M	1850	NUVA	1769.4601	0.15923315	11112.4	13912.1
11476	laaq01_G185	Feige48	G185M	1850	NUVB	1838.1334	0.10789306	17036.6	17829.8
11476	laaq01_G185	Feige48	G185M	1850	NUVB	1854.5784	0.29604081	6264.6	15764.9
11476	laaq01_G185	Feige48	G185M	1850	NUVB	1862.5818	0.17088432	10899.7	18295.3
11476	laaq01_G185	Feige48	G185M	1850	NUVC	1950.1443	0.14004634	13925.0	16215.6
11476	laaq01_G185	Feige48	G185M	1850	NUVC	1957.7327	0.16393000	11942.5	12832.9
11476	laaq01_G185	Feige48	G185M	1850	NUVC	1965.1035	0.13654930	14391.2	21295.5
11476	laaq01_G185	Feige48	G185M	1850	NUVC	1966.5520	0.14737509	13343.90	21743.8
11476	laaq01_G225	Feige48	G225M	2250	NUVA	2143.9527	0.11695401	18331.6	25494.2
11476	laaq01_G225	Feige48	G225M	2250	NUVA	2152.2298	0.12941224	16630.8	24567.1
11476	laaq01_G225	Feige48	G225M	2250	NUVA	2158.1592	0.12246929	17622.0	19775.4
11476	laaq01_G225	Feige48	G225M	2250	NUVA	2161.7356	0.14660251	14745.6	25551.9
11476	laaq01_G225	Feige48	G225M	2250	NUVA	2167.4244	0.08887985	24386.0	21399.8
11476	laaq01_G225	Feige48	G225M	2250	NUVA	2171.5383	0.10983476	19771.0	24566.1
11476	laaq01_G225	Feige48	G225M	2250	NUVB	2244.5817	0.13915092	16130.6	23955.6
11476	laaq01_G225	Feige48	G225M	2250	NUVB	2251.9250	0.10715856	21014.90	26833.1

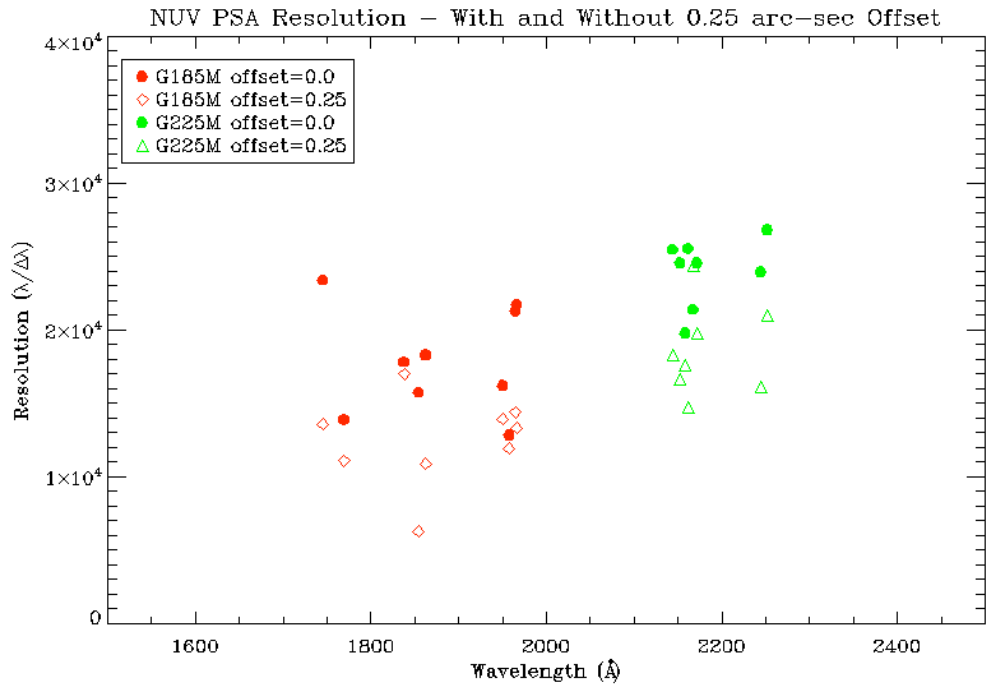

Figure 4-1 Spectral Resolution Degration with target mis-alignment. A 29% and 21% degradation was measured for the G185M and G225M respectively with a 0.25" de-centering of the target in the PSA.

5. On-orbit characterization of the COS NUV Spatial Resolution

Aside from verification of the spectral resolution, the SMOV activities in the NUV included a program to verify the NUV spatial resolution (activity COS-17 "External NUV Spectroscopic Performance - Part II", PID 11477). The other goals of that program were to determine the on-orbit plate scale of the COS NUV channel, to measure the aperture throughput as a function of off-axis position, and to measure the dependence (if any) between the spectral and spatial resolution of the detector.

5.1 Choice of Target

The tests described above should ideally be performed using a pointlike emission line source, in order to isolate and characterize the spatial and spectral profiles as much as possible. In COS 17, we observed three pointlike emission line sources. These included (1) the symbiotic star AG Dra (V=9.8, consisting of a K giant and a white dwarf (T_{eff} ~ 10^5 K)), which was observed during Visit 1 of that program through the PSA aperture with the G185M, G225M and G285M gratings, (2) the symbiotic star He 2-38 (V=13.1; Visit 2), observed through the PSA aperture with G230L, and (3) RR Tel (V=11.4, a slowly evolving symbiotic nova; Visit 3) through the BOA aperture (all NUV gratings).

The observations through the PSA consisted of an exposure with the target centered in the aperture, followed by a series of exposures where the target was offset along dispersion and perpendicular to dispersion. The offsets, specified by the POSTARG parameter, took the source out beyond the edge of the aperture. For the G185M grating observations, the exposures included a set of POSTARG sequences along the dispersion and perpendicular to dispersion. The G225M, G285M and G230L POSTARG sequences, on the other hand, were performed solely perpendicular to dispersion. In all observations through the BOA the target was centered in the aperture.

A summary of the exposures for all targets in program COS-17 observed through the PSA is given in Tables 5-1, 5-2, 5-3 and 5-4. The POSTARG sequences employed in these observations (specified in arcseconds) are indicated in the second column of each table as (X,Y) pairs, with X and Y indicating offsets along dispersion and perpendicular to dispersion, respectively. The observations with the PSA aperture were all obtained at the nominal FP-POS position (FP-POS=3), at central wavelengths of 1900 Å (G185M, t_{exp} = 50 s), 2390 Å (G225M, t_{exp} = 110 s), 2739 Å (G285M, t_{exp} = 70 s) and 2950 Å (G230L, t_{exp} = 360 s). The BOA observations were obtained at central wavelengths of 1900 Å (G185M, t_{exp} = 650 s), 2390 Å (G225M, t_{exp} = 7820 s), 2657 Å (G285M, t_{exp} = 850 s) and 3000 Å (G230L, t_{exp} = 220 s).

5.2 Data Reduction and Analysis

All data for program 11477 were obtained in time-tag mode and processed with CalCOS V2.11b. The pipeline processing of the two-dimensional spectra included corrections for the flat field, dead time, Doppler and heliocentric velocity. The corrected time-tag data are saved as 2-D events tables (**corrtag.fits** file; Kaiser et al. 2008), with separate columns containing the data corrected along dispersion for the Doppler motion of HST, the residual drift of the COS OSM2 during the exposure, and finally the full correction. We utilized the fully corrected columns in our analysis (XFULL and YFULL, corresponding to dispersion and cross-dispersion directions, respectively). We performed all of our analysis using the IDL software contained in the CEDAR package from the University of Colorado. We used CEDAR to display the XFULL and YFULL columns from the corrtag.fits files. For each grating we displayed the XFULL and YFULL columns from the **corrtag.fits** files and chose the brightest emission line for analysis. We fit the profile of each line in both X and Y directions with a Gaussian. Although the COS LSF in the NUV exhibits broad non-Gaussian wings (Ghavamian et al. 2009), using the Gaussian fit should still allow for a reasonably accurate measurement of the line centroids and the identification of any trends in the line profile widths when the source is moved off-center in the PSA aperture. The line centroids and widths obtained for each

fitted profile (Xcenter, Ycenter, XFWHM and YFWHM) are shown in Tables 5-1, 5-2, 5-3 and 5-4.

The spectra of AG Dra and He 2-38 consist of several isolated, prominent emission lines superimposed on a faint, flat continuum. To perform our analysis we chose the brightest of these emission lines for each grating. The lines analyzed from the PSA observations were Si III] 1892 Å (G185M, Stripe B), He II 2733 Å (G225M, Stripe B) and He II 2385 Å (G285M, Stripe B) in AG Dra and C III] 1909 Å (G230L, Stripe C: 2nd order) in He 2-38. The emission line widths along dispersion were ~ 6-20 pixels, significantly larger than the instrumental resolution of 2.5-3 pixels (i.e., the spectral lines were all resolved by COS).

The NUV spectra of RR Tel are dominated by prominent emission lines of Si II 1808 Å, Si III] 1892 Å, CIII] 1909 Å, He II 2385 Å and [Mg V] 2783 Å. A faint underlying continuum is present in all the BOA spectra. The C III] and Si III] nebular lines from the source are known to exhibit widths ~ 35 km s^{-1} while the He II line has a width ~ 70 km s^{-1} (Nussbaumer & Dumm 1995). Based on the BOA spectral resolution measurements in Figure 3-2, we expect the C III] and Si III] lines to be unresolved in the BOA spectra, and the He II line to be marginally resolved. The source is point-like, so it is spatially unresolved. Perpendicular to the dispersion, the emission line profiles in RR Tel exhibit both narrow and broad components. This is the result of the distortion produced by the wedge-like shape of the neutral density filter. The BOA image of a point source exhibits a chevron-like shape with a bright core and flared tail (see Figure 8.5 from the Cycle 18 COS Instrument Handbook). When collapsed along dispersion, the core and tail produce spatial profiles that are well fit by narrow (~2-3 pixels) and broad (~6-9 pixels) Gaussians, respectively. The results of these fits are reported in Table 5-5.

6. On-orbit COS NUV Spatial Resolution Results

6.1 POSTARG-induced Spectral Shifts

The (X,Y) positions of the targeted spectral lines, observed through the PSA (Tables 5-1, 5-2, 5-3 and 5-4) are shown in Figure 5-1. It is clear from the figure that for the medium resolution NUV gratings a positive POSTARG specified perpendicular to the dispersion direction (+ΔY) results in a small negative shift of the spectrum along dispersion (-ΔX), and vice versa for negative POSTARGs. For the medium resolution gratings, the magnitude of the shift increases with increasing POSTARG. In contrast, there is little or no shift observed for the G230L data. There is also negligible shift in the cross-dispersion direction for the medium resolution gratings when a POSTARG is excecuted purely along dispersion. Interestingly, the axes defined by the data points in figure 5-1 are not perpendicular to one another for the M-mode gratings, suggesting that the shifts

cannot be characterized by a simple rotation (as one would get, say, if the gratings were slightly tilted relative to the detector in their position on the OSM). A more detailed study will remain for future work.

Our analysis shows that a specified POSTARG of 0.5″ (≈ 22 pixels) perpendicular to dispersion results in a shift of approximately 3 pixels (approximately one NUV resolution element; 15 km s^{-1}) along dispersion. The COS calibration pipeline currently does not assume any variation of the wavelength solution with cross-dispersion location of the source. The shifts along dispersion may significantly affect extended sources larger than 0.5″ across, where the spatial profile of the source may not drop sharply with position away from the aperture center. In these cases, the widths of emission or absorption lines in the extracted spectrum can be broadened by as much as 1 spectral resolution element when the spectrum is summed perpendicular to dispersion. The broadening effect is less important for extracted spectra of sources larger than 1″ across, since the aperture throughput of the PSA drops sharply beyond 1″ (as will be shown below). For very extended sources, the spectrum of the object becomes less useful beyond 1″ from the aperture center, due to overlap of the different NUV stripes perpendicular to dispersion.

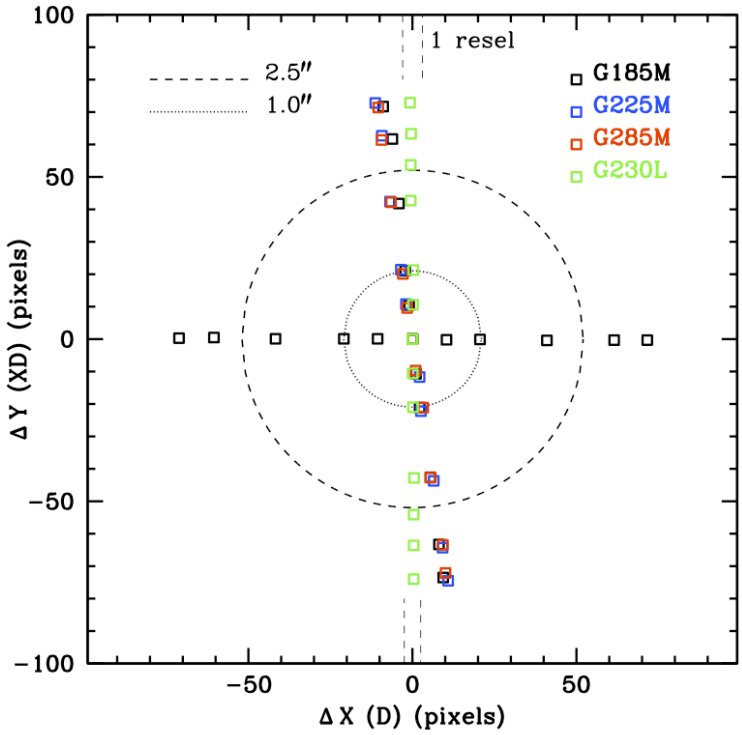

Figure 6-1 Mapping of the offsets introduced in the position of an emission line for observations offset from the center of the PSA aperture. There is a distinct shifting of the emission line centroid along dispersion (ΔX) when non-zero POSTARGs are specified purely along cross-dispersion (ΔY). The width of a 3-pixel NUV resolution element (resel) is marked by the dashed lines at the top and bottom. The size of the PSA (2.5″ diameter) is marked on the Figure by the dashed circle.

Table 6-1. Summary of the files used for the G185M spectral analysis of AG Dra (PID 11477), along with the centroid and width (along dispersion and along cross-dispersion) of the most prominent emission line (Si III] 1892 Å; Stripe B) on the detector.

Filename (*_corrtag.fits)	POSTARG (X,Y) (″)	Ycenter (pix)	YFWHM (pix)	Xcenter (pix)	XFWHM (pix)
labm01c8	(0,0)	287.2	3.2	297.9	6.0
Labm01ca	(0,+0.25)	297.9	3.7	296.9	6.3
labm01cc	(0,+0.50)	308.3	3.1	295.7	6.2
labm01ch	(0,+1.0)	329.0	4.4	293.8	7.0
labm01cj	(0,+1.5)	348.9	3.2	291.8	6.2
labm01cl	(0,+1.75)	358.9	3.5	289.0	7.7
labm01cn	(0,0)	287.9	2.7	297.7	6.2
labm01cp	(0,-0.25)	276.3	2.8	298.8	6.1
labm01cr	(0,-0.50)	265.9	2.7	299.9	6.3
labm01ct	(0,-1.0)	244.4	3.5	303.2	8.2
labm01cv	(0,-1.5)	223.7	3.7	305.8	6.1
labm01cx	(0,-1.75)	213.5	3.3	307.1	6.3
labm01cz	(0,0)	286.8	2.4	298.5	5.7
Labm01d2	(+0.25,0)	286.6	2.8	308.9	6.3
labm01d4	(+0.50,0)	286.7	3.2	319.1	6.3
labm01d6	(+1.0,0)	286.4	4.3	339.5	7.5
labm01d8	(+1.5,0)	286.5	2.8	360.0	7.7
labm01da	(+1.75,0)	286.5	3.1	370.1	5.5
labm01dc	(0,0)	286.7	3.2	298.2	6.2
labm01de	(-0.25,0)	286.8	3.5	287.6	6.5
labm01dg	(-0.50,0)	286.8	3.9	277.3	6.4
labm01di	(-1.0,0)	286.8	4.4	256.5	6.6
labm01do	(-1.5,0)	287.2	2.3	237.7	7.2
labm01dm	(-1.75,0)	287.0	2.5	227.1	7.9

Table 6-2. Summary of the files used for the G225M spectral analysis of AG Dra (PID 11477), along with the centroid and width (along dispersion and along cross-dispersion) of the most prominent emission line (He II 2733 Å; Stripe B) on the detector.

Filename (*_corrtag.fits)	POSTARG (X,Y) (″)	Ycenter (pix)	YFWHM (pix)	Xcenter (pix)	XFWHM (pix)
labm01ee	(0,0)	286.3	2.5	343.1	13.6
Labm01ei	(0,+0.25)	297.1	2.5	341.1	13.8
labm01ek	(0,+0.50)	307.7	2.6	339.5	13.8
labm01em	(0,+1.0)	328.7	3.3	336.2	14.3
labm01eo	(0,+1.5)	349.0	3.5	333.7	13.3
labm01eq	(0,+1.75)	359.1	4.0	331.7	15.1
labm01es	(0,0)	287.4	2.2	343.0	16.1
labm01eu	(0,-0.25)	275.7	2.1	345.2	14.1
labm01ew	(0,-0.50)	265.2	2.3	345.6	13.9
labm01ey	(0,-1.0)	243.7	4.2	349.5	16.4
labm01f0	(0,-1.5)	223.1	3.7	352.2	16.8
labm01f2	(0,-1.75)	212.9	4.2	353.9	21.1
labm01f4	(0,0)	286.3	2.4	343.0	15.0

Table 6-3. Summary of the files used for the G285M spectral analysis of AG Dra (PID 11477), along with the centroid and width (along dispersion and along cross-dispersion) of the most prominent emission line (He II 2385 Å; Stripe B) on the detector.

Filename (*_corrtag.fits)	POSTARG (X,Y) (″)	Ycenter (pix)	YFWHM (pix)	Xcenter (pix)	XFWHM (pix)
labm01dq	(0,0)	299.3	2.2	370.4	13.6
Labm01ds	(0,+0.25)	308.9	2.3	368.8	12.7
labm01du	(0,+0.50)	319.4	2.4	367.5	13.3
labm01dw	(0,+1.0)	341.5	3.3	363.9	13.1
labm01dy	(0,+1.5)	360.7	3.9	361.0	13.7
labm01e0	(0,+1.75)	370.7	4.6	360.0	13.0
labm01e2	(0,0)	298.2	2.2	370.2	14.0
labm01e4	(0,-0.25)	288.5	2.3	371.2	13.2
labm01e6	(0,-0.50)	277.1	2.4	373.5	13.0
labm01e8	(0,-1.0)	255.5	3.9	375.7	14.2
labm01ea	(0,-1.5)	234.8	4.6	379.5	11.3
labm01ec	(0,-1.75)	226.1	6.1	380.3	12.1

Table 6-4. Summary of the files used for the G230L spectral analysis of He 2-38 (PID 11477), along with the centroid and width (along dispersion and along cross-dispersion) of the most prominent emission line (C III] 1909 Å; Stripe C) on the detector.

Filename (*_corrtag.fits)	POSTARG (X,Y) (″)	Ycenter (pix)	YFWHM (pix)	Xcenter (pix)	XFWHM (pix)
labm02wc	(0,0)	176.8	2.8	616.6	2.6
Labm02we	(0,+0.25)	187.4	3.3	616.8	3.1
labm02wg	(0,+0.50)	198.1	3.4	616.9	3.4
labm02wi	(0,+1.0)	219.5	4.6	616.1	4.5
labm02wk	(0,+1.25)	230.5	6.3	616.1	4.7
labm02wm	(0,+1.50)	240.1	4.2	616.2	3.5
labm02wv	(0,+1.75)	249.7	4.4	615.9	3.3
labm02wx	(0,0)	176.9	2.8	616.7	2.6
labm02wz	(0,-0.25)	166.3	3.7	616.8	3.4
labm02x1	(0,-0.5	155.9	4.0	616.9	3.9
labm02x3	(0,-1.0)	134.1	4.7	617.2	5.3
labm02x5	(0,-1.25)	122.8	5.6	617.1	5.0
labm02x8	(0,-1.50)	113.3	3.8	617.1	3.1
labm02xa	(0,-1.75)	102.9	4.3	617.1	3.8
labm02xc	(0,0)	176.9	3.0	617.2	2.6

Table 6-5. Summary of the files used for BOA spectra analysis of RR Tel (PID 11477), along with the centroids and width (along cross-dispersion) of the strongest emission lines.

Filename	Grating	CENWAVE (Å)	Stripe	Line ID (Å)	YFWHM (Narrow) (pix)	Peak (Narrow) (counts)	YFWHM (Broad) (pix)	Peak (Broad) (counts)
labm03hd	G185M	1900	B	[CIII] 1909	3.4	209.9	6.6	83.1
…	…	…	…	[Si III] 1892	3.6	96.7	7.2	40.9
…	…	…	A	[Si II] 1808	3.5	36.6	7.7	15.5
labmo3hp	G225M	2390	A	[He II] 2306	3.3	51.2	6.4	16.4
…	…	…	B	[He II] 2385	2.9	60.9	8.6	23.5
labm03hh	G285M	2657	C	[Mg V] 2785	3.4	137.4	6.6	58.7
…	…	…	…	[Mg II] 2795	2.9	29.4	6.1	14.5
labm03hl	G230L	3000	A	[C III] 1909	2.8	68.2	9.0	36.3
…	…	…	…	[Si III] 1892	1.9	25.2	8.1	21.0

6.4 NUV Plate Scale Results

We can utilize the shifts computed from the spectra to calculate the plate scale of the COS NUV detector for the four gratings. Since the offsets are specified in arcseconds (POSTARG) and the shifts are recorded in pixels, we can obtain the plate scale by dividing the two quantities. Each POSTARG gives a separate measurement of the plate scale, as well as a measure of the relationship between shifts in the dispersion and cross-dispersion directions.

The dependence between dispersion and cross-dispersion shifts can be characterized via the following pair of equations:

$$\Delta Y_{pix} = \alpha_{YY}\,\Delta Y''_{POSTARG} + \alpha_{YX}\,\Delta X''_{POSTARG}$$
$$\Delta X_{pix} = \alpha_{XY}\,\Delta Y''_{POSTARG} + \alpha_{XX}\,\Delta X''_{POSTARG} \qquad (1)$$

Where $\Delta X''$ and $\Delta Y''$ are the specified POSTARG shifts along dispersion and along cross-dispersion in arcseconds, and ΔX_{pix} and ΔY_{pix} are the resulting shifts on the NUV detector in pixels. The α factors are the plate scale coefficients in units of pixels/arcsecond. The subscripts on the coefficients can be interpreted in the following way: α_{XY} is the pixel shift along dispersion produced by a specified POSTARG of 1″ along cross-dispersion, and so on. The coefficients α_{XX} and α_{YY} are then the plate scales along dispersion and perpendicular to dispersion, respectively. For a given emission line, the coefficients can be estimated separately for each exposure (i.e., each POSTARG). The average of the coefficients for each grating is shown in Table 6-6. The derived coefficients are within 10% of what was predicted by simulations with the Target Acquisition Analysis for COS (TAACOS) program (COS-11-0024).

Table 6-6. Plate scale coefficients derived for the COS NUV detector. These can be used with Equation (1) to predict the spectral shift for positions offset from the center of the PSA aperture.

Plate scale (pixels/″)	G185M	G225M	G285M	G230L
α_{YY}	42.0	43.2	41.0	41.7
α_{YX}	-0.3	…	…	…
α_{XY}	-4.7	-6.7	-5.9	-0.2
α_{XX}	41.3	…	…	…

6.5 Aperture Throughput of the NUV Channel: Results

The flux in the brightest emission line for each grating (the lines used are listed in Section 5.2) was utilized to measure the aperture throughput of the NUV channel. Using the gross counts at the peak of the line and the line FWHM (pixels) recorded in our Gaussian, we measured the variation of the quantity (FWHM × peak) to quantify the decline in flux as a function of off-axis position. Normalizing these quantities to the on-center value, we produced the throughput curve shown in Figure 6-2. As can be seen in the curves and the vertical dash lines in Figure 6-2, the NUV aperture throughput at the edge of the PSA aperture is ~ 40% of the on-center value for the medium resolution gratings. The throughput is significantly lower at the edge of the aperture for the G230L grating (only ~ 25% of central value). The throughput remains close to the maximum value for positions within 0.5" of the aperture center.

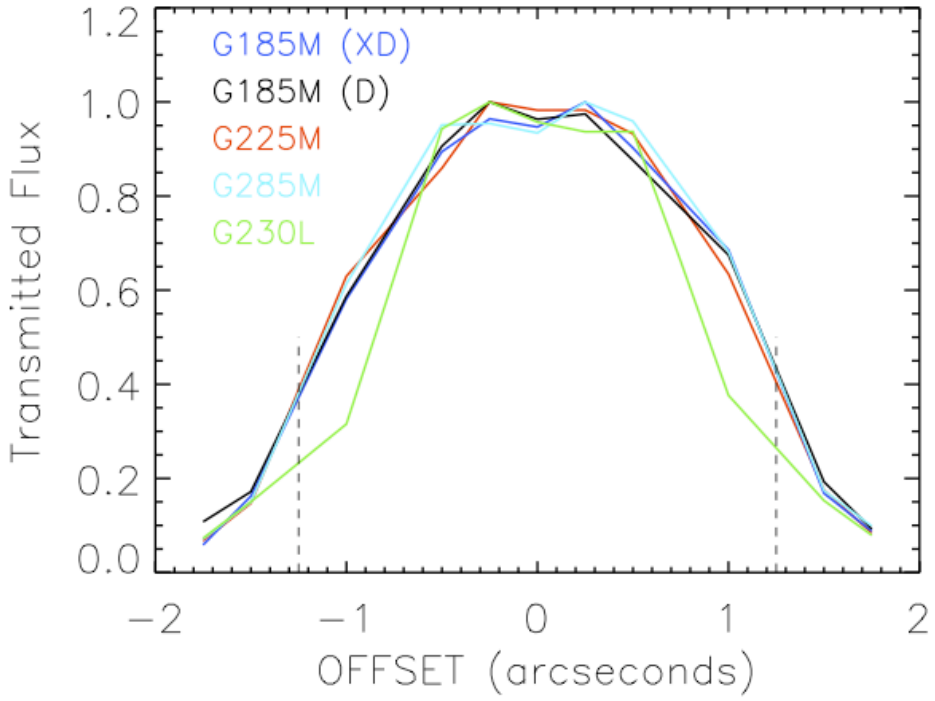

Figure 6-2. The PSA aperture throughput of the COS NUV channel, shown as a function of off-axis position. For G185M the results are shown both along the dispersion (D) and perpendicular to dispersion (XD). The edge of the aperture (2.5" across) is marked by the dotted line.

6.6 Spatial Resolution of the NUV Channel: Results

The spatial resolution of NUV channel in spectroscopic mode can be characterized by the FWHM of the source perpendicular to dispersion (the column marked YFWHM in Tables 6-1 through 6-4). From the plate scales stated in Table 6-5 and the line widths listed in

Tables 6-1 to 6-4, we estimate the following spatial resolution for PSA observations in the four medium resolution gratings: 0.068 ± 0.010" (G185M), 0.055" ± 0.003" (G225M), 0.054" ± 0.002" (G285M) and 0.069" ± 0.003" (G230L). The medium resolution values are consistent with each other to within the errors, with the low resolution grating having a lower spatial resolution than the other three gratings. Note that these estimates do not take into account the uncertainty in the NUV plate scale (~10%) or other systematic uncertainties.

We used the two-component Gaussian fits to emission lines in RR Tel to estimate the NUV spatial resolution with the BOA aperture. For each emission profile we calculated the flux-weighted FWHM for the broad and narrow components along the cross-dispersion direction, using values from Table 6-6. We then averaged the flux-weighted FWHM values for all the emission lines in a given spectrum. For the four NUV gratings we obtain a BOA spatial resolution of approximately 0.29″, 0.22″, 0.24″ and 0.38″ for G185M, G225M, G285M and G230L, respectively.

7. Summary

For all COS NUV gratings, the spectral resolution for data taken through the PSA aperture meets the CEI requirements. For the BOA, we found a good match between the ground estimates of the resolution (derived from the imaging mode data), and the measurements from this SMOV program (derived by comparing spectral line widths with STIS spectra). There are no CEI specifications for the resolution through the BOA. The spatial resolution of the NUV channel is consistent with thermal vacuum measurements, while the plate scale of the NUV channel is consistent with prelaunch simulations. On-orbit measurements of the aperture throughput show that the flux transmitted through the PSA is nearly constant within 0.5" of the aperture center.

8. Change History for COS ISR 2010-08

Version 1: September 30 2010

9. References

- COS IDT, "Cosmic Origins Spectrograph (COS) Science Operations Requirements Document (OP-01)," (2003)
- COS IDT, "COS Pre-Launch Calibration Data" Document (AV-04)," (2008)
- COS IDT, "TAACOS: Phase I NUV Report" (COS-11-0024) (2001)
- "Hubble Space Telescope Cosmic Origins Spectrograph Contract End Item (CEI) Specification" (STE-63) (2004)
- Nussbaumer, H. & Dumm, T. 1997, A&A 323, 387
- Soderblom, D. R., et al. 2007, "The Cosmic Origins Spectrograph Instrument Handbook, version 1.0", (Baltimore, STScI)
- Heber, U. Reid, I. N., Werner, K. 2000, A&A, 363, 198
- O'Toole, S. J., Heber, U., Benjamin, R. A. 2004, A&A, 422, 1053
- Ghavamian, P. et al. 2009, COS ISR 2009-01
- Kaiser, M. B. et al. 2008, SPIE 7014, 70146G-1

Acknowledgments

The authors would like to thank Tony Keyes and Steven Penton for helpful discussions.

AG Dra is an irregularly variable symbiotic star, capable of producing bright enough outbursts to damage the FUV detectors on COS. The observations of AG Dra were made possible by over six weeks of nightly ground bases monitoring leading up to our exposures. This support was performed by the Asiago Novae and Symbiotic stars (ASN) Collaboration led by Ulisse Munari and the American Association of Variable Star Observers (AAVS). We thank the members of these teams for their dedicated and patient assistance in ensuring the safety and schedulability of the SMOV observations.